Numerical Study of Unsteady non-Newtonian Viscoelastic Flow in a 2D "T" Junction

H.M.M. Matos[1], P.J. Oliveira[1]

[1] Unidade de Materiais Têxteis e Papeleiros, Depto. de Engenharia Electromecânica. Universidade da Beira Interior (Portugal).

Introduction

A computational fluid dynamics simulation study has been carried out for unsteady laminar flow in a planar 2D T-junction, using non-Newtonian viscoelastic fluids with characteristics similar to those of blood. In the large blood vessels, blood can be modelled as a Newtonian fluid, however in smaller vessels it exhibits non-Newtonian behaviour, showing a shear-thinning viscosity and, additionally, it is thixotropic and viscoelastic [1, 2].

The present study aims at quantifying the effect of elasticity on the main flow characteristics in a dividing T-junction geometry, namely the size of the two recirculation zones created near the bifurcation, where vascular diseases like the formation of atherostic plaques and thrombi can occur [3]. The variation of elasticity is achieved by varying the Deborah number ($De = \lambda u / H$) for a constant extensibility and polymer concentration.

The study is thus a first attempt to apply viscoelastic rheological models in bifurcation flows such as those which are relevant in hemodynamics.

Numerical Simulation

Differential equations

For an incompressible flow, the equations to be solved are those expressing conservation of mass (Eq. (1)) and linear momentum (Eq. (2)):

$$\nabla \bullet \boldsymbol{u} = 0 \qquad (1)$$

$$\frac{\partial \rho \boldsymbol{u}}{\partial t} + \nabla \bullet (\rho \boldsymbol{u}\boldsymbol{u}) = -\nabla p + \nabla \bullet \boldsymbol{\tau} + \nabla \bullet (2\eta_S \boldsymbol{D}) \qquad (2)$$

In these equations $\boldsymbol{u}$ is the velocity, p is the pressure, ρ is the fluid density, $\boldsymbol{D}$ is the rate-of-strain tensor and η_S is the solvent viscosity.

For the evaluation of the stress tensor in Eq. (2) we use a rheological constitutive model derived from kinetic theory for finite extensibility non-linear dumbbells. In the FENE-CR model proposed by Chilcot and Rallison [4], the fluid has constant viscosity but shear-thinning relaxation time. The stress tensor is obtained from:

$$\boldsymbol{\tau} + \lambda \left(\frac{\overset{\triangledown}{\boldsymbol{\tau}}}{f(\boldsymbol{\tau})} \right) = 2\eta_p \boldsymbol{D} \qquad (3)$$

λ is the relaxation time of the fluid at zero shear rate, the symbol $\triangledown$ denotes the Oldroyd upper convected derivative and the function $f(\boldsymbol{\tau})$ is given by:

$$f(\boldsymbol{\tau}) = (L^2 + (\lambda / \eta_p) tr(\boldsymbol{\tau})) \big/ (L^2 - 3) \qquad (4)$$

where L^2 is the extensibility parameter (here $L^2 = 100$) and tr represents the trace operator.

Numerical Method

The differential equations described before are discretised using a fully implicit FVM with the collocated variable arrangement [5]. Spatial discretisation of the convective terms is accomplished with the high resolution scheme CUBISTA [6]. For the temporal discretisation of

the unsteady term we follow the three time level scheme [7]. The pressure-correction algorithm employed is based on the SIMPLEC algorithm.

Geometry and computational mesh.

The simulations were carried out in a 2D T-shaped geometry (Fig.1) having a constant cross-section area with height H.

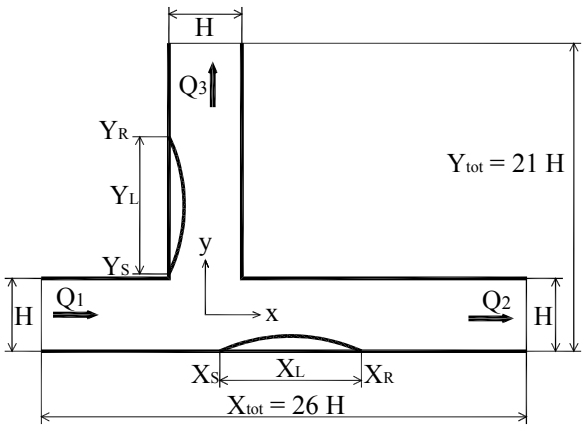

Figure 1. Schematic representation of the test section.

The flow conditions were similar to those of Khodadadi [8] and Miranda et al. [2]. At the inlet (X= -3.5) a pulsating flow with a sinusoidal shape was imposed, generated by an sinusoidal pressure gradient:

$$-\frac{dp}{dx} = \rho K_S + \rho K_0 \cos(\omega t) \qquad (4)$$

The Reynolds number based on the steady bulk flow is 102, the ratio of oscillating and steady pressure gradients $K_0/K_S = 2.585$, the Womersley number $\alpha = (H(\omega/\nu)^{1/2}) = 4.864$, the flow rate ratio is $Q_3/Q_1 = 0.7$, the retardation ratio $\beta = \eta_S/\eta = 0.9$, where $\eta = \eta_S + \eta_P$ is the total viscosity of the fluid and η_P is the polymeric viscosity.

At the outlets, Neumann boundary conditions were imposed. Other boundary planes of the geometry, except inlet and outlet planes, correspond to solid walls where the no slip boundary condition was imposed. The mesh used in this work is the same of Matos et al. [9] where a study of mesh refinement can be found. The mesh is formed by 12800 control volumes and is orthogonal but non-uniform, with minimum space 2.5×10^{-4}, while the time step is 5×10^{-3}.

Results and Discussion

All results are normalised, using the height at inlet H for length scale, 1/3 of the wall shear stress for stresses and $2\pi/\omega$ for time scale. Fig. 2 shows the variation for a complete cycle of the separation (X_S, Y_S) and reattachment (X_R, Y_R) points of the horizontal and vertical recirculations (cf. Fig. 1) for the FENE-CR viscoelastic fluid at De=5.

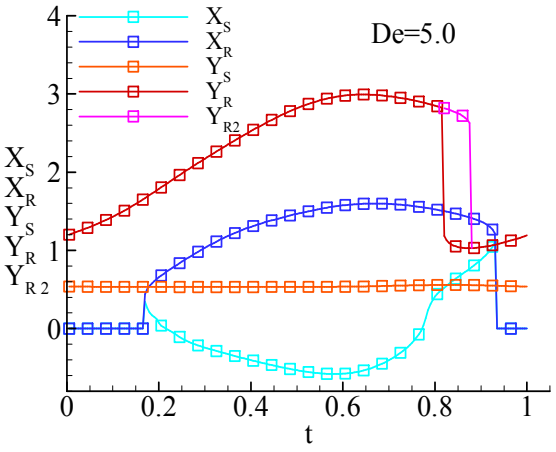

Figure 2. Location of recirculations (viscoelastic fluid, De=5).

It is observed that the horizontal recirculation is not present during the whole cycle, and that its increase in length is both due to the upstream movement of the separation point and the downstream movement of the reattachment point. One the other hand, the vertical recirculation is always present during the cycle and, as expected, the separation point is always situated very close to the upstream corner of the T. An abrupt reduction in the length of the vertical recirculation occurs at $t \approx 0.8$, which is associated with the break up of the recirculation into two vortices (cf. [2]); the red line corresponds to the first reattachment point (unique before the division) and the purple line to the second reattachment point associated with a second recirculation that tends to disappear later in the cycle (Fig. 3).

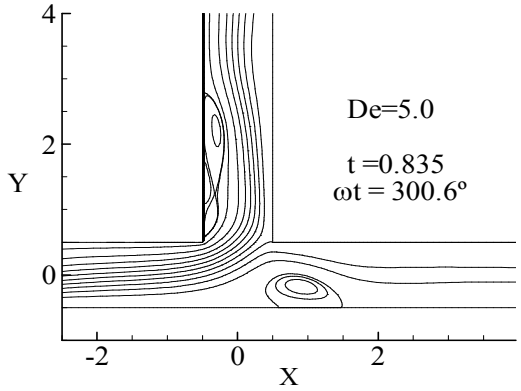

Figure 3 .Streamlines for De=5 and ωt=300.6º.

Figs. 4 and 5 show the variation of the recirculation lengths with an increase in fluid elasticity. The results for the recirculation in the main duct (Figs. 4) indicate a decrease of vortex size with the increase of elasticity; the maximum difference registered between Newtonian and viscoelastic cases (De=10) is 18.7% at t=0.61.

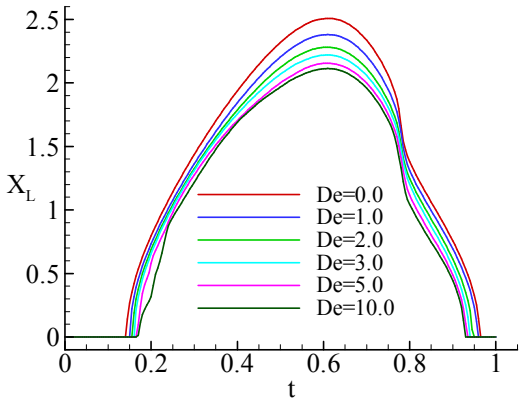

Figure 4. Horizontal recirculation length with increased elasticity.

Fig. 4 also shows a delay of the starting point and an advance of the end point of the horizontal recirculation, with the increase of De, resulting in recirculations with lower periods of residence during the cycle. The maximum variation is 20.7% for the separation and 3.8% for the reattachment points of the recirculation.

In the branching duct the variation of the recirculation length is less pronounced and does not exhibit a monotonic variation with the increase of elasticity during the whole cycle. At the beginning of the cycle the variation is linear and the length decreases with the increase of elasticity; however when the maximum length is achieved ($t \approx 0.64$), the length tends to increase to a maximum for De=3.0 and decrease for larger values of De. At this point the maximum variation present between the Newtonian and the De=3.0 cases is only 1%.

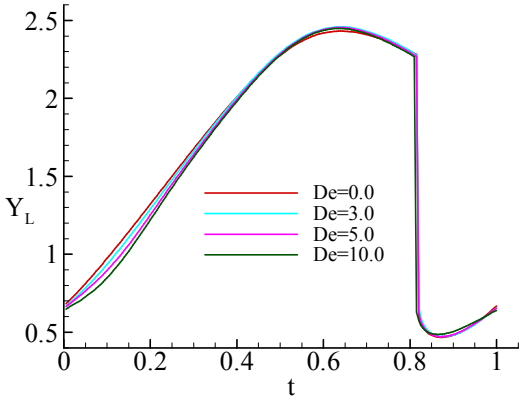

Figure 5. Vertical recirculation length with increased elasticity.

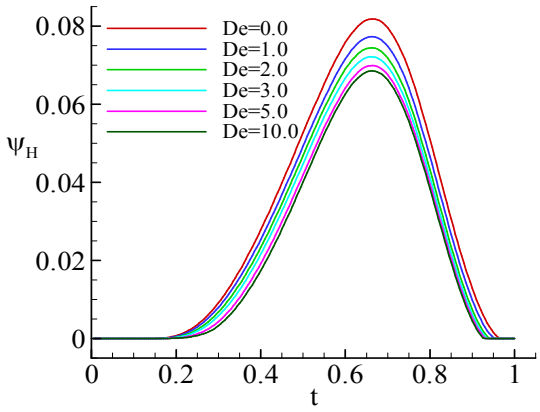

Figure 6. Vortex intensity in the horizontal recirculation for increased elasticity.

The intensity of both recirculations shows an behaviour similar to the size variation during the cycle: increasing when the recirculation size is increasing and vice-versa. Fig. 6 shows the variation of the vortex intensity for the horizontal recirculation as a function of elasticity, for a cycle. From this figure we observe a decrease of the vortex intensity with elasticity and a maximum variation of 19.4% at t=0.665. Similar trends were observed for the vertical recirculation, with a maximum variation of 4.7% in intensity at t=0.62.

Figures 7 and 8 show the evolution of the shear stress along two horizontal profiles, at the bottom (Y=-0.5) and top walls (Y=+0.5) in the main duct,

and two vertical profiles, at the proximal (X=-0.5) and distal walls (X=+0.5) in the branching, for a 90 deg phase angle. The shear stress for the viscoelastic case represents only the polymeric part, which explains the differences between the Newtonian and viscoelastic cases. In the latter case, a solvent contribution with a similar shape to the Newtonian results must be added to the polymeric contribution

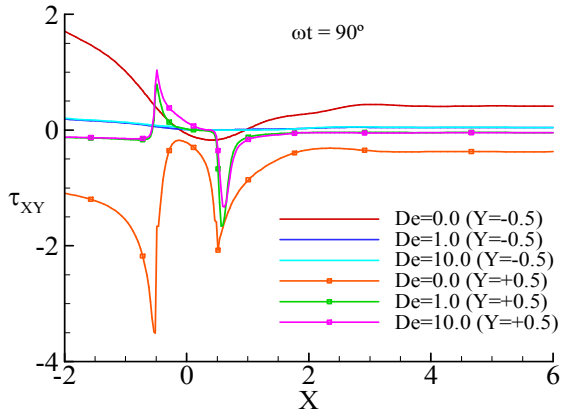

Figure 7. Shear stress along the bottom and top walls.

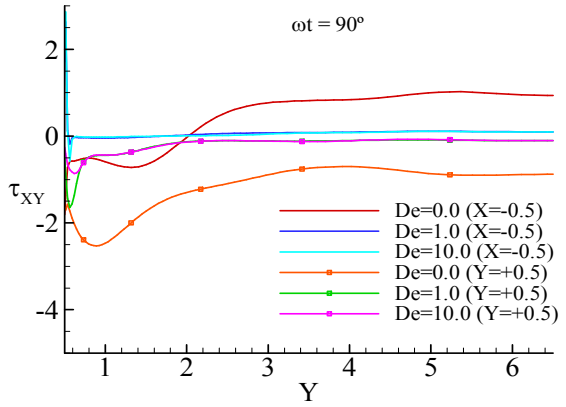

Figure 8. Shear stress along the proximal and distal walls.

Both figures show low shear stresses in the recirculation zones for the bottom and proximal walls, but very high shear stress are registered at the re-entrant corners which is in agreement with the literature. An increase of elasticity tends to increase the shear stress field; however between the re-entrant corner at X=-0.5 and the bifurcation centre (Fig. 7), a distinct behaviour was observed for Newtonian and viscoelastic cases, with elasticity tending to decrease the shear stress field.

Concluding Remarks

From the results presented, concerning the influence of elasticity upon unsteady flow in a T-junction, it is concluded that in general elasticity tends to decrease the length and intensity of the recirculations, while it tends to increase the shear stresses.

Acknowledgements

To Fundação para a Ciência e Tecnologia (FCT) through grant SFRH/BD/18062/2004 and project POCTI/EME/58657/2004.

References

1. Owens, R.G. (2006). J. non-Newtonian Fluid Mech. 140, 57-70.
2. Miranda, A.I.P., Oliveira, P.J., and Pinho, F.T. (2008). Int. J. Numer. Meth. Fluids 57, 295-328.
3. Ku, D. (1997) *Annual Review of Fluid Mech.* 29, 399-434.
4. Chilcot, M.D., and Rallison, J.M. (1988). J. non-Newtonian Fluid Mech. 29, 381-432.
5. Oliveira, P.J., Pinho, F.T., and Pinto, G.A. (1998). Int. J. Numer. Meth. Fluids 79, 1-43.
6. Alves, M.A., Oliveira, P.J., and Pinho, F.T. (2003). Int. J. Numer. Meth. Fluids 41, 47-75.
7. Oliveira, P.J. (2001). J. non-Newtonian Fluid Mech. 101, 113-137.
8. Khodadadi, J.M. (1991). J. Fluids Eng. 113, 111-115.
9. Matos, H.M.M., Alves, M.A., and Oliveira, P.J. (2007). in CMNE/CILANCE 2007 (Sá, J.C. et al. eds.), pp. 365, APMTAC/FEUP, Porto.

Contact Address:

Paulo Jorge Oliveira (pjpo@ubi.pt)
Departamento de Engenharia Electromecânica.
Universidade da Beira Interior,
6200-001 Covilhã (Portugal)
Telf.: +351 275329946; Fax: +351 275329972;